JCTC Journal of Chemical Theory and Computation

Article

Cite This: J. Chem. Theory Comput. 2018, 14, 3252−3261

pubs.acs.org/JCTC

Coarse-Grained Force Field for Imidazolium-Based Ionic Liquids

Alireza Moradzadeh, Mohammad H. Motevaselian, Sikandar Y. Mashayak, and Narayana R. Aluru*

Department of Mechanical Science and Engineering, Beckman Institute for Advanced Science and Technology, University of Illinois at Urbana−Champaign, Urbana, Illinois 61801, United States

Supporting Information

ABSTRACT: We develop coarse-grained force fields (CGFFs) for computationally efficient and accurate molecular simulation of imidazolium-based ionic liquids. To obtain CGFF parameters, we employ a systematic coarse-graining approach based on the relative entropy (RE) method to reproduce not only the structure but also the thermodynamic properties of the reference all-atom molecular model. Our systematic coarse-graining approach adds a constraint to the RE minimization using the Lagrange multiplier method in order to reproduce thermodynamic properties such as pressure. The Boltzmann inversion technique is used to obtain the bonded interactions, and the non-bonded and long-range electrostatic interactions are obtained using the constrained relative entropy method. The structure and pressure obtained from the coarse-grained (CG) models for different alkyl chain lengths are in agreement with the all-atom molecular dynamics simulations at different thermodynamic states. We also find that the dynamical properties, such as diffusion, of the CG model preserve the faster dynamics of bulky cation compared to the anion. The methodology developed here for reproduction of thermodynamic properties and treatment of long-range Coulombic interactions is applicable to other soft-matter.

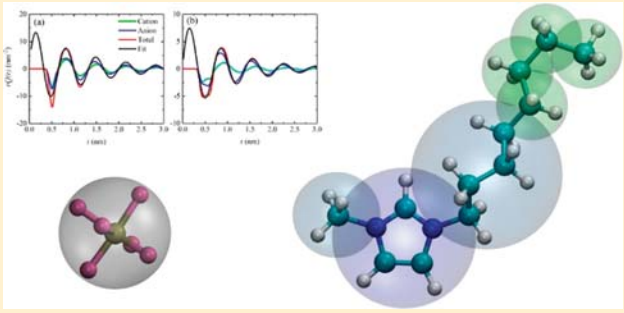

1. INTRODUCTION

Room-temperature ionic liquids (RTILs) are an emerging class of solvents primarily composed of organic cations and inorganic anions. Due to their structural complexity, they are in a liquid state at room temperature. RTILs have distinct properties distinguishing them from conventional electrolytes with uniform charge density dissolved in a large amount of solvent or high-temperature molten salts. Their emergence has opened new avenues for many industrial and scientific applications such as energy storage in non-Faradaic batteries, electrotunable friction, drug discovery, and gas capture.[1−5] Due to a variety of cations and anions, an unlimited number of RTILs can be engineered for various applications, thereby making them "designer solvents". However, a lack of fundamental understanding of their structural and dynamical behavior hinders numerous potential applications of the RTILs.

The emergence of advanced computational resources has allowed researchers to use molecular dynamics (MD) simulations to study many biological and physicochemical systems at the nanoscale.[6] MD simulation of RTILs has attracted wide attention as it can shed light on the physical mechanisms governing their behavior.[7−13] MD simulations, for example, are performed to understand the short lifetime of ion pairs.[4] In addition to MD simulations, using a combination of molecular and multiscale coarse-grained (CG) simulations, it was shown that the neutral tail of cations tends to aggregate heterogeneously, while the charged head groups of RTILs distribute uniformly in order to minimize electrostatic interaction within the system.[14−18] Even though MD simulations led to advances in the performance and fundamental understanding of physical phenomena in various applications like the electrochemical double-layer (ECDL) capacitor and drug delivery, many profound questions still remain to be answered concerning RTILs physical and chemical behavior.[2,10,19−23]

The mesoscale study of many systems using classical MD simulation is hindered by its computational cost. Therefore, CG models are proposed in order to bridge the length scales for many phenomena.[24−26] MD simulation of RTILs at the mesoscale, which requires simulating a large system of hundreds of thousands of atoms for a long time (micro- to milliseconds), becomes computationally intractable, especially because of their slow dynamics. Because of the aforementioned benefits of coarse graining, development of CG models has been an active area of research. Two different routes are pursued to develop CG models, namely, top-down and bottom-up approaches. In the top-down strategy, the interactions are parametrized with simple analytical potential forms, and the parameters in the potentials are determined by reproducing macroscopic thermodynamic properties obtained from experiments or simulations. This approach typically involves minimal information regarding the underlying all-atom (AA) model and usually leads to inaccurate structural representation.

In the bottom-up approach, the essential information of the AA system is included during the CG model development. The

Received: December 28, 2017
Published: May 11, 2018

DOI: 10.1021/acs.jctc.7b01293
J. Chem. Theory Comput. 2018, 14, 3252−3261

main challenge in systematically developing CG models is to incorporate the average effects of the detailed system into a CG representation with reduced degrees of freedom. During the last two decades, several attempts have been made to address this issue.[27−30] The methods are usually based on reproducing the structural properties or forces of an AA reference system. Voth et al. proposed the force matching method, and it has been successfully applied to various soft matter systems such as synthetic and biological systems.[14,24] On the other hand, methods such as the iterative Boltzmann inversion (IBI) and inverse Monte Carlo reproduce the structure.[31−34] CG methods, however, suffer from problems such as transferability and representability. For example, a CG model which reproduces the structure of an AA system is not guaranteed to preserve other thermodynamic properties of the reference system such as pressure, energy, and free energy of solvation.[35] In general, the CGFFs work well for the objectives they are optimized for it. Due to the reduced number of degrees of freedom and the smoother potential landscape, the time step for integrating the equations of motion in coarse-grained molecular dynamics (CGMD) simulations is several times higher than the reference AAMD simulation, thereby allowing simulation of systems at larger time and length scales.

Another challenge in the parametrization of CGFFs is to systematically take into account the long-range interactions in a high-resolution atomistic system into a low-resolution representation (CG model). Most of the CG methods rely on the modification of the short-range pairwise potential in order to implicitly consider the effects of electrostatic interactions.[17] Recently, there have been attempts to consider the electrostatic interaction explicitly as it is an ubiquitous driving force in a variety of biomolecular phenomena including protein folding and DNA−protein assembly to mention a few.[36−39] In the case of RTILs, Dong et al. calculated that 70% of the interaction energy in RTILs is of Coulombic nature, even though hydrogen-bonding and van der Waals interactions play important roles in the structure and behavior of RTILs.[40] Furthermore, recent studies showed that the net charges of cations and anions can have significant effects on the behavior of RTILs.[41] Thus, arbitrary reduction of charges should be avoided during parametrization of AA and CG force fields in order to keep all interactions consistent with the reference system. We systematically link the long-range Coulombic interactions between CG and AA models using total Coulombic interactions calculated based on the particle mesh Ewald[42] method. In RTILs, many phenomena occurring at meso- and macro-scale arise due to their nanostructure organization,[43,44] therefore using a structure-based CG model can be considered as an attractive approach for multiscale study of RTILs. Furthermore, multiscale studies using CGMD simulation are a reliable method to understand many physical phenomena including charge dynamics mechanisms in nanopores[3,45,46] and formation of micelles in aqueous solution of RTILs and membrane disruption of bilayers, multilayers, and vesicles by RTILs.[47−49]

CG model development for RTILs, has been extensively studied.[4,13,16] The force matching technique, for example, has been applied by Wang et al. to develop a CG model for $[EMIM]^+[NO_3]^-$.[17] Since then, there have been many attempts to develop CG models for various RTILs like $[EMIM]^+[BF_4]^-$ and $[BMIM]^+[BF_4]^-$ using different algorithms.[46] Wang et al. introduced an effective force CG model (EF-CG) for imidazolium-based nitride ionic liquids with various alkyl-chain lengths.[16] They showed that by sacrificing some accuracy in the radial distribution function (RDF), it is possible to obtain a general force field that is transferrable to different temperatures and various side-chain lengths. Wang et al. used IBI and inverse Monte Carlo methods to develop structure-based CG model for $[EMIM]^+[PF6]^-$.[50] The study concluded that the presence of explicit charges on the interacting sites results in a more transferable and realistic force field; however, a systematic determination of optimal charges remains unclear. Top-down CGFFs of RTILs have also been developed to reproduce thermodynamic and dynamical properties. Bhargava et al. introduced a CGFF for $[BMIM]^+[PF_6]^-$, using initial values for CGFF parameters based on the mapped atom interaction parameters, including charges and Lennard-Jones (LJ) energy and diameter.[48] The method relies on scaling the parameters until the desired properties[51] are reproduced. Roy et al. introduced two CG models based on reproducing density and diffusion of $[BMIM]^+[PF_6]^-$, using the standard 12-6 LJ potential form and charge reduction. However, the CG parameters are obtained by hand tuning, focusing on matching dynamical and thermodynamic properties of RTILs and not their structure.[52,53] This model has been successfully used to study many physical phenomena occurring in supercapacitors. Nevertheless, the optimal CG parameters, especially charges, are not obtained systematically, and the procedure is somewhat ad hoc. Using the same approach, Merlet et al. reproduced the thermodynamic and dynamical properties for $[EMIM]^+[BF_4]^-$ and $[BMIM]^+[BF_4]^-$ in the bulk and near graphene interfaces.[54] In spite of prior studies to develop CG models for ILs, the main shortcoming of these models is the determination of optimal charges and interaction parameters to reproduce structure and pressure at the same time.[55]

In our framework, the charge of the CG bead is a scaled sum of the charges of the atoms mapped into a CG bead, where the scaling factor is optimized within the relative entropy (RE) framework. Furthermore, by employing the Lagrange multiplier constraint optimization method, we minimize the relative entropy objective function such that it reproduces the pressure of the AA system. By doing so, the resultant CGFF can be used for simulations in the isothermal−isobaric ensemble (NPT).

In this paper, we investigate the development of a general CGFF for 1-butyl-3-methylimidazolium hexafluorophosphate ionic liquid and longer alkyl chains with systematic consideration of the long-range interaction and pressure matching within the RE framework. The remainder of the paper is organized as follows: First, we describe the CG model development including the treatment of the long-range interaction and pressure-matching technique. Then, the transferability and representability of CGFF are investigated for different thermodynamic states and longer chain imidazolium ionic liquids through calculation of different properties such as pair and charge radial distribution functions and density.

2. COARSE-GRAINED MODEL DEVELOPMENT

In this study, we develop CGFFs for imidazolium-based cation and hexafluorophosphate anion ionic liquids ($[C_nC_1IM]^+[PF_6]^-$). The minimum chain length we consider in this study is four ($n \geq 4$). As we employ bottom-up coarse-graining, the information from the fine-grain system is collected from the AAMD simulations of $n = 4$ and $n = 8$ (details of the AAMD and CGMD simulations are given in the Supporting Information Section S1).

DOI: 10.1021/acs.jctc.7b01293
J. Chem. Theory Comput. 2018, 14, 3252−3261

For the CG model development, the atoms of the AA system are lumped into five types of CG beads as shown in Figure 1 for

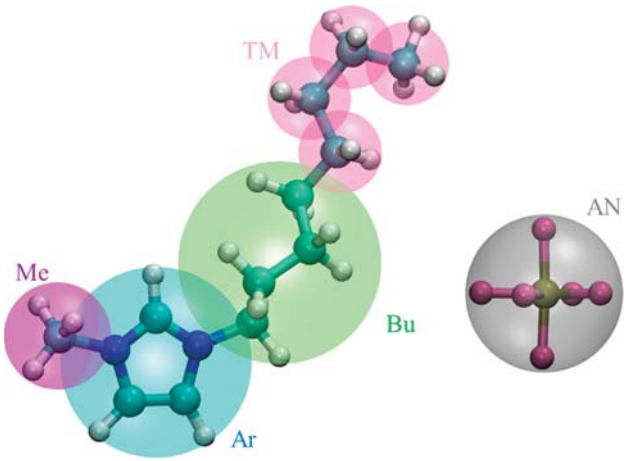

Figure 1. Schematic representation of AA and CG molecular structures. All-atom and CG representation of cation for n = 8.

$[C_8C_1IM]^+$ $[PF_6]^-$. The structure of the CG model is chosen in accordance with previous studies including CG, united-atom, and AA models as well as AAMD results of current study,[13,52−54] while attempting to decrease the degrees of freedom as much as possible (details are given in Tables S1−S3 of the Supporting Information). Due to the fact that anion has a rotational symmetry and behaves as a rigid body, we map it to a single CG bead (AN). In a similar manner, considering the rotational symmetry in the methyl group near the aromatic ring, it is grouped as one CG bead (Me). The backbone of the aromatic ring in the cation also moves as a rigid body, so it is considered as one CG bead (Ar). The butyl group near the aromatic ring is considered as another CG bead (Bu) as shown in Figure 1. The methyl and methylene groups at the tail of the alkyl chain are considered as one type of CG bead (TM) mainly because of simplicity of the CG model and its compatibility with the underlying AA force field. Table 1

Table 1. Bond, Angle, and Dihedral Types for Cation

	atoms	type		atoms	type
1	Me-Ar	bond	7	Bu-TM-TM	angle
2	Ar-Bu	bond	8	TM-TM-TM	angle
3	Bu-TM	bond	9	Me-Ar-Bu-TM	dihedral
4	TM-TM	bond	10	Ar-Bu-TM-TM	dihedral
5	Me-Ar-Bu	angle	11	Bu-TM-TM-TM	dihedral
6	Ar-Bu-TM	angle	12	TM-TM-TM-TM	dihedral

shows bond, angle, and dihedral types in the CG representation, and this definition ensures the generality and applicability of the current CGFF to shorter and longer alkyl chains. In the CGFF development, we first optimize the non-bonded interactions of $[C_4C_1IM]^+[PF_6]^-$ system. For $n > 4$, we further optimize those interactions created by the addition of the TM beads. In order to determine the bonded interactions, we study $[C_8C_1IM]^+[PF_6]^-$ as it contains all of the possible conformational distributions (bond, angle, and dihedral angle distributions).

The CGFF is comprised of non-bonded and bonded interactions, and the total potential energy can be written as

$$U_{total} = U_{nb} + U_b \tag{1}$$

where U_{nb} is the energy of the non-bonded interactions between the CG beads, and U_b denotes the bonded potential energy. The non-bonded potential includes the summation of the short-range van der Waals (u_{vdW}) and the long-range Coulombic pair potentials (u_{Coul}). The non-bonded interactions are considered for beads in different molecules or beads within a molecule with at least three bonds apart. We consider two forms of short-range vdW interactions: uniform cubic B-splines (SP) and standard 12-6 LJ. In the case of a SP pair potential, an interval from zero to a cutoff distance, R_{cut}, is discretized into $n - 1$ segments, $\{r_0, r_1, r_2, ..., r_{n-1}\}$, of equal size $\Delta r = R_{cut}/(n - 1)$ such that $r_i = i \times \Delta r$, where $i \in (0, ..., n - 1)$. The value of the SP pair potential at a distance r can be written as follows

$$u_{sp}(r) = [1\ t\ t^2\ t^3]\frac{1}{6}\begin{bmatrix} 1 & 4 & 1 & 0 \\ -3 & 0 & 3 & 0 \\ 3 & -6 & 3 & 0 \\ -1 & 3 & -3 & 1 \end{bmatrix}\begin{bmatrix} c_j \\ c_{j+1} \\ c_{j+2} \\ c_{j+3} \end{bmatrix} \tag{2}$$

where $\{c_0, c_1, c_2, ..., c_{n+1}\}$ are the spline knot values, and the index j is determined such that $r_j \le r < r_{j+1}$ and t is given by

$$t = \frac{r - r_j}{\Delta r} \tag{3}$$

For the LJ potential, we use the standard 12-6 form as

$$u_{LJ}(r) = \frac{C_{12}}{r^{12}} - \frac{C_6}{r^6} \tag{4}$$

where $C_{12}(= 4\epsilon\sigma^{12})$ and $C_6(= 4\epsilon\sigma^6)$ are interaction parameters, in which ϵ and σ are energy- and length-scale parameters for the LJ interaction, respectively. The long-range Coulombic interaction is given by

$$u_{Coul}(r_{ij}) = A_c\frac{q_iq_j}{4\pi\epsilon_0 r_{ij}} \tag{5}$$

where q is the net lumped charge of the AA system in the CG representation, ϵ_0 is the permittivity of vacuum, and A_c is a charge scalar factor applied to the Coulombic interactions in the CGFF. The bonded interactions include only angle and dihedral terms among the beads of the same molecule. All bonds are assumed to be rigid and constrained using the LINCS algorithm. Based on the previous studies and AAMD simulations of the current study, for short chain imidazolium-based IL (n = 4), the angle is kept constant.[52,54,56] For longer chain ILs, we use the Boltzmann inversion to obtain the dihedral and angle interactions. For this purpose, we assume that angle, and dihedral angle probability distributions are not correlated, that is,

$$P(\theta, \phi) = P_{angle}(\theta)P_{dihedral}(\phi) \tag{6}$$

where θ and ϕ denote angle and dihedral angle, respectively. The resultant potentials are obtained using the Boltzmann inversion of the target probability distributions, which are computed using MD trajectories. Thus,

$$U_{nb} = -k_BT\sum_{q=\theta,\phi} \ln P(q) \tag{7}$$

DOI: 10.1021/acs.jctc.7b01293
J. Chem. Theory Comput. 2018, 14, 3252−3261

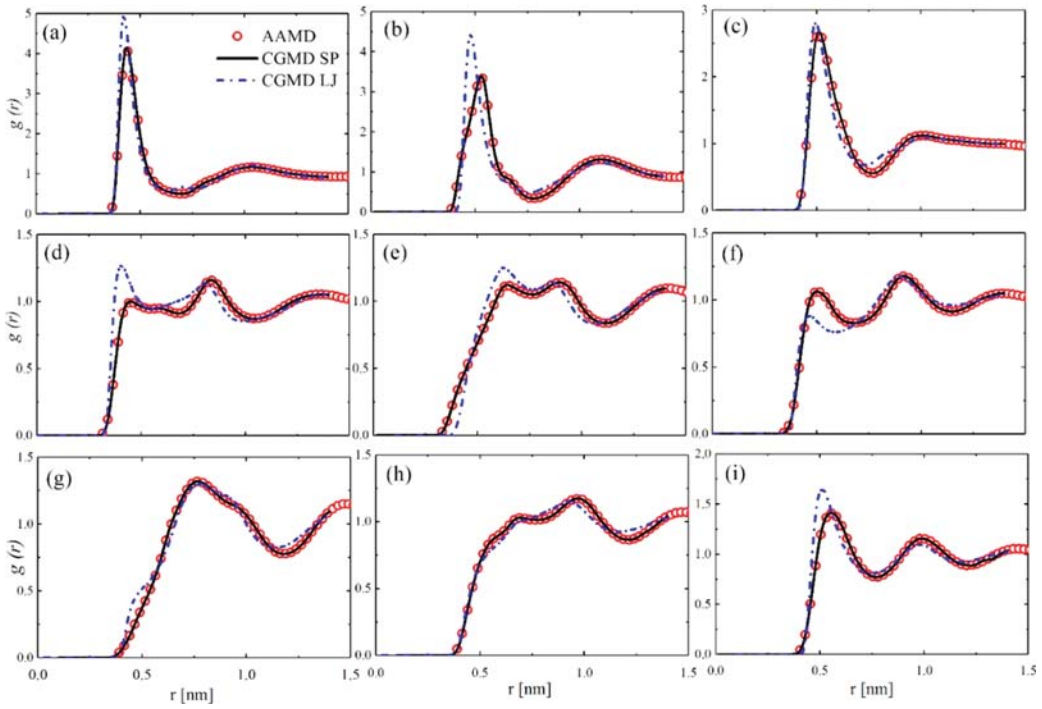

Figure 2. Bead−Bead RDF of C_4MIM. (a) AN-Me, (b) AN-Ar, (c) AN-Bu, (d) Me-Me, (e) Me-Ar, (f) Me-Bu, (g) Ar−Ar, (h) Ar-Bu, and (i) Bu-Bu. Strong short-range correlation between oppositely charged beads is present in the first row, while for similar charges the short-range correlation is weak and almost close to 1.0 even though long-range correlation exists for both of them. Circles are AAMD, black solid line is CGMD-SP, and blue dash dot line is CGMD-LJ.

where q represents a degree of freedom, which can be either θ or ϕ. The probability distributions are given in Figures S1 and S2 of the Supporting Information.

The only interaction parameters to be optimized are the non-bonded interactions and the charge scalar factor. In the case of the SP pair potential, we optimize the knot values (c_j), while in the LJ form, the optimization parameters are C_{12} and C_6. To optimize the non-bonded parameters, we use the constrained relative entropy (CRE) minimization. Originating from the information theory, the RE method is used to quantify overlap between two molecular ensembles.[57] Through RE, it is possible to connect AA and CG ensemble averages and such a relation can be written as follows

$$S_{\mathrm{rel}} = \sum_i p_{\mathrm{AA}}(r_i) \ln\left(\frac{p_{\mathrm{AA}}(r_i)}{p_{\mathrm{CG}}(M(r_i))}\right) + \langle S_{\mathrm{map}}\rangle_{\mathrm{AA}} \tag{8}$$

where the summation proceeds over all the configurations of the reference AA system, $\boldsymbol{r} = \{r_i\}(i = 1,2, ...)$, $M(r)$ is the mapping operator from AA to CG configuration, S_{map} is the mapping entropy that originates from degeneracies in the AA model mapping, and $p_{\mathrm{AA}}(r_i)$ and $p_{\mathrm{CG}}(M(r_i))$ are the normalized probability of a configuration i in the AA and CG ensembles, respectively. In the canonical ensemble, the RE simplifies to

$$S_{\mathrm{rel}} = \beta\langle U_{\mathrm{CG}} - U_{\mathrm{AA}}\rangle_{\mathrm{AA}} - \beta\langle F_{\mathrm{CG}} - F_{\mathrm{AA}}\rangle_{AA} + \langle S_{\mathrm{map}}\rangle_{\mathrm{AA}} \tag{9}$$

where all the averages are computed in the reference AAMD ensemble, F is the configurational part of the Helmholtz free energy, and U is the total energy of the system. In this study, the total potential energy of the CG system is given by

$$U_{\mathrm{CG}} = U_{\mathrm{nb}} + \sum_{j>i}\sum_{i=1}^{N}\left(u_{\mathrm{Coul}}(r_{ij}) + u_{\mathrm{vdW}}(r_{ij})\right) \tag{10}$$

Note that the first term in eq 10 is not a function of the optimization parameters. In this study, in addition to the short-range interactions, we include optimization of the Coulombic interactions through a charge scalar factor, A_c. The current approach can pave way for more systematic consideration of the Coulombic interactions in developing the CGFFs, as they play a key role in many physicochemical and biological processes. The details regarding calculation of different quantities in CG and AA ensembles are given in Chaimovich and Shell.[27] The optimization parameters ($\boldsymbol{\lambda}$) include the knot values or the LJ parameters as well as the charge parameter A_c. In the original RE formulation,[58] the Newton−Raphson strategy is used to obtain the optimal parameters, and they are iteratively refined using the following equation:

$$d\boldsymbol{\lambda} = -\mathbf{H}_{S_{\mathrm{rel}}}^{-1}\cdot\nabla_{\boldsymbol{\lambda}} S_{\mathrm{rel}} \tag{11}$$

where $d\boldsymbol{\lambda}$ is the change of parameters based on the previous iteration. The original RE, formulated in the canonical ensemble, does not guarantee that the pressure of the AA system is preserved, because both the virial and the kinetic parts of the pressure in the CG system are different from the target system. Prior work has suggested several methods to reproduce the pressure of the AA system, and these methods usually rely on the addition of the pressure correction terms, constrained optimization of CG parameters, or a volume-dependent contribution to the potential.[32,59−61] In this study, we employ CRE minimization with Lagrange multiplier to reproduce the pressure of the AA system.[62] In a molecular system, the pressure is given by

DOI: 10.1021/acs.jctc.7b01293
J. Chem. Theory Comput. 2018, 14, 3252−3261

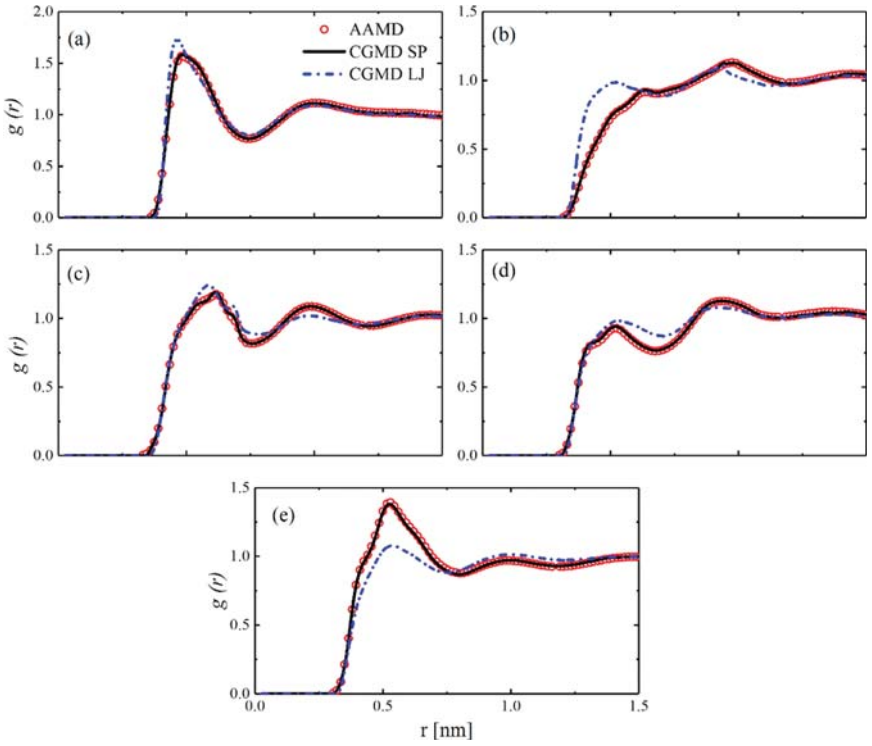

Figure 3. Bead−Bead RDF of C_8MIM for interactions between new bead and other beads. As the new bead is neutral, the correlations are weak. (a) AN-TM, (b) Ar-TM, (c) TM-Bu, (d) TM-Me, and (e) TM-TM.

$$P = \frac{1}{V}\left(\frac{1}{3}N_{\mathrm{DOF}}k_{\mathrm{B}}T + \left\langle \frac{1}{3}\sum_{j>i}\mathbf{f}_{ij}\cdot\mathbf{r}_{ij}\right\rangle\right) \tag{12}$$

where N_{DOF} is the number of degrees of freedom in the system, and V is the volume of the simulation box. The second term in eq 12 is the virial part of the pressure and $\mathbf{f}_{ij}$ is the force between two beads, i and j. The mathematical description of the Lagrange multiplier is presented in Section S2 of the Supporting Information. Therefore, the CRE is defined as follows

$$S_{\mathrm{crel}} = \beta\langle U_{\mathrm{CG}} - U_{\mathrm{AA}}\rangle_{\mathrm{AA}} - \beta\langle A_{\mathrm{CG}} - A_{\mathrm{AA}}\rangle_{\mathrm{AA}} + \langle S_{\mathrm{map}}\rangle_{\mathrm{AA}} + \chi g(\boldsymbol{\lambda}) \tag{13}$$

where $g(\boldsymbol{\lambda})$ is the constraint, and χ is the Lagrange multiplier. The CRE optimization for pressure-matching and long-range Coulombic interactions is implemented in the VOTCA package.[63,64] The constraint and parameter refinements can be written as

$$g(\boldsymbol{\lambda}) = \frac{1}{2}\left(\frac{P_{\mathrm{CG}}(\boldsymbol{\lambda}) - P_{\mathrm{AA}}}{P_{\mathrm{AA}}}\right)^2 \tag{14}$$

$$d\boldsymbol{\lambda}^{c} = d\boldsymbol{\lambda} + \mathbf{H}_{S_{\mathrm{rel}}}^{-1}\mathbf{J}^{T}\cdot(\mathbf{J}\cdot\mathbf{H}_{S_{\mathrm{rel}}}^{-1}\mathbf{J}^{T})^{-1}(g(\boldsymbol{\lambda}) + \mathbf{J}\cdot d\boldsymbol{\lambda}) \tag{15}$$

where P_{CG} and P_{AA} are the pressure in CG and AA systems, respectively, and $\mathbf{J}$ is the Jacobian and is given by

$$\mathbf{J} = \left(\frac{P_{\mathrm{CG}} - P_{\mathrm{AA}}}{P_{\mathrm{AA}}^2}\right)\frac{\partial P_{\mathrm{CG}}}{\partial \boldsymbol{\lambda}} \tag{16}$$

where

$$\frac{\partial P_{\mathrm{CG}}}{\partial \boldsymbol{\lambda}} = \frac{1}{3V}\left\langle \frac{\partial}{\partial \boldsymbol{\lambda}}\sum_{n<m}\left(r_{nm}\frac{du_{\mathrm{CG}}(r)}{dr}\bigg|_{r=r_{nm}}\right)\right\rangle_{\mathrm{CG}} \tag{17}$$

3. RESULTS AND DISCUSSION

The LJ CG parameters are given in Tables S4−S6 of the Supporting Information. The corresponding tables (LJ and SP potentials) necessary for CGMD simulations are provided in the Supporting Information. In order to investigate the representability and transferability of the developed CGFF, we carry out CGMD and AAMD simulations of ILs for different thermodynamic states and alkyl chain lengths. The structural properties such as pair and charge radial distribution functions of both AA and CG models are compared with each other. The thermodynamic and dynamical properties are computed using the CGFF and are determined for different thermodynamic states and longer chain ILs.

3.1. Structural Properties. In order to quantify the structural properties obtained from AA and CG systems, we evaluate RDFs between different beads and the center of mass (COM) of the cation (CA) and the anion (AN) in both systems. For both AA and CG systems, the RDFs between different pairs in $[C_4C_1IM]^+[PF_6]^-$ and $[C_8C_1IM]^+[PF_6]^-$ systems at the reference T = 400 K are shown in Figures 2 and 3, respectively.

The short-range correlation between the oppositely charged CG beads is strong, which can be related to the strong attractive electrostatic interactions between them (Figure 2a−c). The RDF profiles show long-range correlation, which persists even beyond 1.5 nm. This phenomenon can be attributed to the presence of long-range electrostatic interactions and heterogeneous structure in RTILs.

DOI: 10.1021/acs.jctc.7b01293
J. Chem. Theory Comput. 2018, 14, 3252−3261

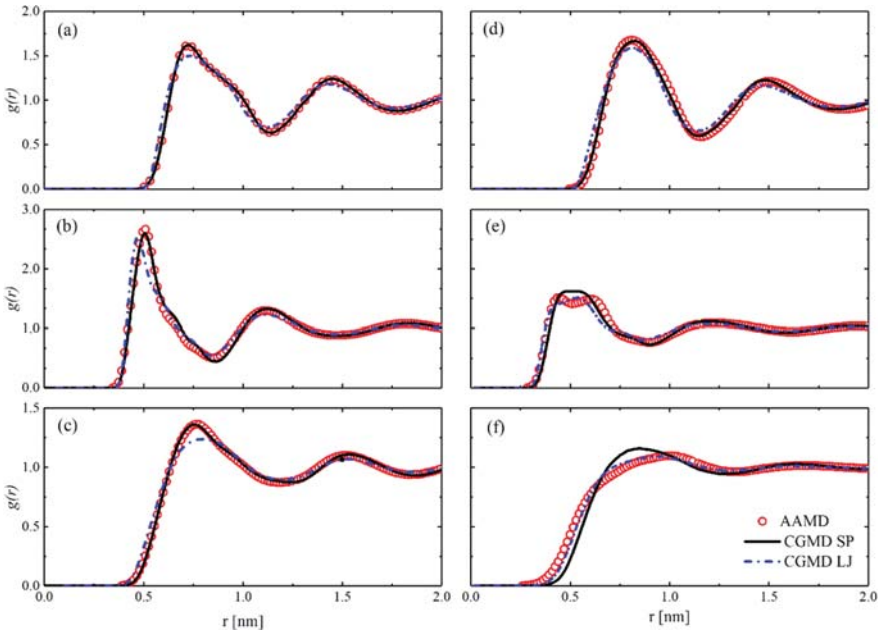

Figure 4. Structural properties of the center of mass from AAMD and CGMD. (a–c) AN-AN, CA-AN, and CA-CA RDF for C_4MIM. (d–f) AN-AN, CA-AN, and CA-CA RDF for C_8MIM.

The COM RDFs are shown in Figure 4. It can be seen that the CGMD simulations are able to capture structural properties of both C_4MIM and C_8MIM. For example, the coordination numbers in both AAMD and CGMD are shown in Table 2, and

Table 2. Coordination Number Obtained from AAMD and CGMD Simulations for C_4MIM and C_8MIM

	n = 4			n = 8		
C_nC_1IM PF_6	CA-CA	CA-AN	AN-AN	CA-CA	CA-AN	AN-AN
AAMD	6.87	2.52	5.89	2.72	3.25	6.19
CGMD-SP	6.91	2.58	5.89	2.05	3.22	6.11
CGMD-LJ	6.91	2.60	5.81	2.03	3.21	6.02

they are in good agreement with each other. Moreover, it can be seen from Figure 4 that the short-range correlation becomes much weaker as the alkyl-chain increases. This is more evident in case of the CA-AN RDF (see Figure 6). This can be attributed to the decrease in the screening length of the Coulombic interactions.

In this study, we use charge-ordering to further investigate screening in RTILs. Previous AAMD and CGMD calculations have shown charge-ordering in RTILs.[50,52] The charge radial distribution, $Q_i(r)$, can be defined such that $4\pi r^2 q_i Q_i(r)dr$ is the net charge from a central ion i of charge q_i at a distance r. The following relations can be written between the charge radial distribution and RDFs of cation–cation (CA-CA), cation–anion (CA-AN), and anion–anion (AN-AN):

$$Q^{CA}(r) = \rho(g^{CA\text{-}CA}(r) - g^{CA\text{-}AN}(r)) \quad (18)$$

$$Q^{AN}(r) = \rho(g^{AN\text{-}AN}(r) - g^{CA\text{-}AN}(r)) \quad (19)$$

$$Q(r) = Q^{CA}(r) + Q^{AN}(r) \quad (20)$$

where ρ is the total number density of ions ($\rho = \rho_{cation} + \rho_{anion}$). In Figure 5, the oscillatory behavior of charge in both $[C_4C_1IM]^+[PF_6]^-$ and $[C_8C_1IM]^+[PF_6]^-$ systems are shown.

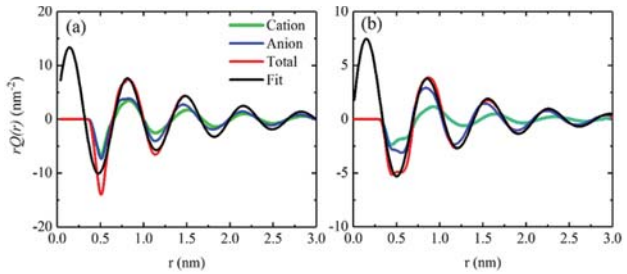

Figure 5. Charge distribution functions calculated for C_4MIM and C_8MIM at 400 K. The fit has been used to find the screening lengths, which are found to be 1.19 and 1.03 nm for (a) C_4MIM and (b) C_8MIM, respectively.

According to Keblinski et al.,[65] the asymptotic form of the charge distribution function approaches the general form of eq 21 at high ionic strength:

$$Q(r) = \frac{A}{r} e^{-r/\lambda_{IL}} \sin\left(\frac{2\pi r}{d} + \psi\right) \quad (21)$$

where A is the amplitude of exponentially decaying charge–charge correlations, d and ψ are the period of oscillation and the phase shift, respectively, and λ_{IL} is the screening length, which determines the distance beyond which the local charge neutrality exits. There is no unique screening length for RTILs in the literature. Del Pópolo and Voth[18] calculated a screening length of 0.7 nm for $[EMIM]^+[NO_3]^-$. There are two values reported for $[BMIM]^+[PF_6]^-$ (1.45 and 2.5 nm from studies by Roy et al.[53] and Wang et al.,[50] respectively). In the latter study, they use AAMD, while in the former study, CGMD was used. In this study, we use a larger system compared with the previous studies.[53] According to our fit in Figure 5, the screening length for C_4MIM and C_8MIM are 1.19 and 1.03 nm, respectively. In addition, the results from longer chain ionic liquid provide a far more accurate picture regarding screening

DOI: 10.1021/acs.jctc.7b01293
J. Chem. Theory Comput. 2018, 14, 3252–3261

length in ionic liquid solutions, especially as this topic has been the focus of many prior studies.[66,67]

Due to the simplicity of eq 21, it provides only a qualitative behavior of RTILs which are highly structured liquids. Our results indicate that the screening length of RTILs decreases with an increase in the alkyl chain length, which is expected as the heterogeneity of the system increases due to the interaction between the alkyl chains. Furthermore, alkyl chain interactions decrease the correlation due to the Coulombic interactions, thereby decreasing the screening length. We calculate these parameters using the CGMD simulation for $n = \{4, 6, 8, 10\}$. The results are provided in Figure 6.

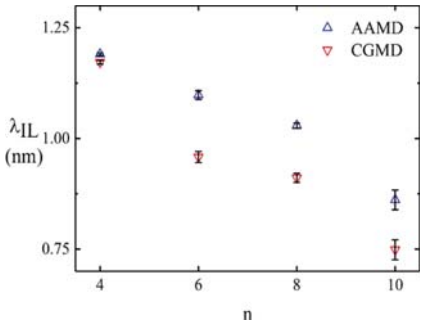

Figure 6. Screening length of ILs as a function of alkyl-chain length.

3.2. Thermodynamic and Dynamical Properties.

Thermodynamic and dynamical properties obtained from bottom-up CGFF are usually different compared with those obtained from the reference AAMD simulations. It is, however, possible to add correction to the interactions in order to reproduce several properties.[30,68] In this study, we use CRE minimization to reproduce pressure of AAMD simulation. We also study transferability and representability of the CGFF to obtain other thermodynamic and dynamical properties at different thermodynamic states and varying alkyl chain lengths.

3.2.1. Density. The CRE approach developed here is expected to reproduce the target pressure and density in the isothermal−isobaric ensemble. Therefore, we study transferability and representability of CGFF parameters by calculating density of CGMD simulation in the NPT ensemble for different alkyl-chains and at different thermodynamic states. Tables 3 and 4 show the results obtained from AAMD and CGMD for different temperatures and alkyl-chains, respectively. Densities obtained from CGMD simulations are in good agreement with those obtained from AAMD simulations with a maximum relative error of about 3% compared with AAMD results.

3.2.2. Thermal Expansion and Compressibility Coefficients. We compare the thermal expansion coefficients obtained from the CGMD simulation with experimental values. The thermal expansion coefficient is defined as

$$\alpha = \frac{1}{V}\left(\frac{\partial V}{\partial T}\right)_P \approx -\left(\frac{\ln(\rho_2/\rho_1)}{T_2 - T_1}\right)_P \tag{22}$$

where ρ is the density obtained from CGMD simulations. The thermal expansion coefficients are determined based on the densities provided in Table 3. In a similar manner, we also evaluate the isothermal compressibility based on the densities at $P = 1$ atm and $P = 100$ atm, using the following equation:

$$\kappa_T = -\frac{1}{V}\left(\frac{\partial V}{\partial P}\right)_T = \frac{1}{\rho}\left(\frac{\partial \rho}{\partial P}\right)_T = \left(\frac{\partial \ln(\rho)}{\partial P}\right)_T \approx \left(\frac{\ln(\rho_2/\rho_1)}{P_2 - P_1}\right)_T \tag{23}$$

The computed values along with the experimental data are given in Table 5. The derivative quantities like thermal expansion and isothermal compressibility coefficients are harder to reproduce from MD simulation and show higher dependency on the packing as mentioned in previous studies.[13,69] Furthermore, CG model representability problem for different quantities stems from the state dependency of potential of mean force as noted by many previous studies.[70,71] In general, matching pressure between CG and AA models leads to deviation of compressibility obtained from AA and CG models.[59]

3.3. Diffusion Coefficient.

Transport properties of RTILs play a crucial role in many microscopic and macroscopic phenomena, especially in slit pores, where the diffusion can be 1−2 orders of magnitude smaller than bulk or even faster compared to bulk.[73−75] Diffusion is also of significant importance in the charge dynamics of ECDL capacitors.[19] MD simulations provide the trajectories of the molecules from which diffusion coefficients can be extracted. The diffusion coefficient can be determined using the Einstein relation:

$$D = \frac{1}{6}\lim_{t\to\infty}\frac{d}{dt}\langle|\Delta\mathbf{r}(t)|\rangle^2 = \frac{1}{6}\lim_{t\to\infty}\frac{d}{dt}\langle|\mathbf{r}(t) - \mathbf{r}(0)|\rangle^2 \tag{24}$$

where the diffusion coefficient is the mean slope of the mean-squared displacement as time goes to infinity. Figure 7 shows

Table 4. Transferability of CGFF for Different Alkyl-Chain Lengths Based on the Number Density

C_nC_1IM PF_6	n	4	6	8	10
AAMD	density	2.71	2.33	2.05	1.75
CGMD SP	density	2.71	2.27	2.05	1.77
	relative error	(0.00%)	(2.64%)	(0.00%)	(1.14%)
CGMD LJ	density	2.69	2.26	2.05	1.78
	relative error	(0.6%)	(3.00%)	(0.00%)	(1.71%)

Table 3. Transferability of CGFF for a Temperature Range of 300−450 K[a]

	C_4C_1IM PF_6, ρ (nm^{-3})			C_8C_1IM PF_6, ρ (nm^{-3})		
T (K)	AAMD	CGMD SP	CGMD LJ	AAMD	CGMD SP	CGMD LJ
300	2.89	2.82 (2.31%)	2.93 (1.51%)	2.20	2.13 (3.18%)	2.22 (0.91%)
350	2.80	2.76 (1.21%)	2.81 (0.44%)	2.13	2.09 (1.88%)	2.14 (0.47%)
400	2.71	2.71 (0.00%)	2.69 (0.6%)	2.05	2.05 (0.00%)	2.05 (0.00%)
450	2.62	2.65 (1.14%)	2.58 (1.64%)	1.98	2.01 (1.52%)	1.97 (0.51%)

[a]Number density for C_4 and C_8 at different temperatures obtained from CGMD simulations using SP and LJ pair potentials.

DOI: 10.1021/acs.jctc.7b01293
J. Chem. Theory Comput. 2018, 14, 3252−3261

Table 5. Thermal Expansion (α) and Isothermal Compressibility (κ_T) Coefficients Obtained from CGMD Simulation and Compared with Experimental Values[a] (ref 72)

	$C_4C_1IM\ PF_6$				$C_8C_1IM\ PF_6$			
	exp.	AAMD	CGMD SP	CGMD LJ	exp.	AAMD	CGMD SP	CGMD LJ
$\alpha \times 10^{-4}$, K^{-1}	5.95	6.54	4.1	8.5	5.80	7.09	3.9	8.0
κ_T, GPa^{-1}	0.498	0.455	0.85	1.97	0.491	0.971	0.71	1.17

[a]The experimental thermal expansion and isothermal compressibility coefficients are obtained at temperatures of 343.2 and 323.2 K for C_4 and C_8, respectively.

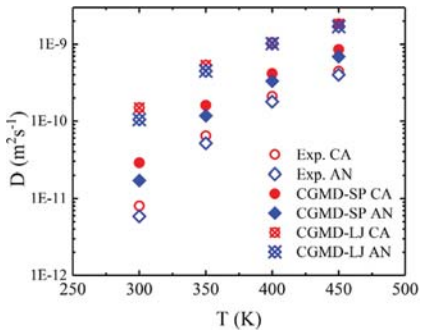

Figure 7. Comparison of diffusion coefficient between the experiment[80] and CGMD simulations as a function of temperature for C_4MIM.

the diffusion coefficient of C_4MIM obtained from CGMD simulations and experiments. CGFFs usually lead to faster dynamics as many degrees of freedom are removed and the free energy landscape is smoothened out during the coarse-graining process. There have been attempts to reproduce the underlying reference dynamics in CGFFs.[76−79] The values obtained using SP pair potentials are in a better agreement with the experimental values compared to the LJ functional form. This can be explained from the more accurate free energy landscape reproduced by using the B-spline potential. Even though the diffusion coefficients are higher for the SP and the LJ potentials compared to the experimental values by a factor of 2 and 5 times, respectively, they capture the faster dynamics of bulky cations compared to anions, which can be related to high charge concentration on anions. CGFF with similar structural behavior and physically consistent transport properties is of significant importance in understanding many physical phenomena such as charge dynamics.

4. CONCLUSION

We have systematically developed a structure-based coarse-grained force field (CGFF), for simulation of imidazolium-based ionic liquids, which has a good transferability across different chain lengths. The force field is developed using constrained relative entropy (CRE) minimization method in order to reproduce structure and thermodynamic property such as pressure. The structure of ionic liquids and charge ordering are investigated using both AAMD and CGMD simulations. Representability of CGFF for other thermodynamics properties is investigated by computing diffusion coefficient, thermal expansion, and compressibility coefficients. The density obtained from the CG model shows a maximum error of 3% for various thermodynamic states and alkyl chain lengths. The compressibility and thermal expansion coefficient deviate (by a factor of 2) from the experimental value, indicating that the pressure constraint does not necessarily guarantee accuracy of other thermodynamics properties. Compared the experimental value, the diffusion coefficient is overestimated by a factor of 2 and 5 times for the SP and the LJ potentials, respectively. However, the faster dynamics of bulky cations compared to anion are captured by the CG model, which demonstrates that the dynamical properties of the system are qualitatively reproduced.

■ ASSOCIATED CONTENT

Supporting Information

The Supporting Information is available free of charge on the ACS Publications website at DOI: 10.1021/acs.jctc.7b01293.

Potential parameters and running file for GROMACS are provided for C8 both in LJ and B-Spline form in order to facilitate simulation and later usage (ZIP)

Bonded distributions and the mathematical description of Lagrange multiplier (PDF)

■ AUTHOR INFORMATION

Corresponding Author

*E-mail: aluru@illinois.edu.

ORCID

Alireza Moradzadeh: 0000-0003-3355-7086

Sikandar Y. Mashayak: 0000-0002-9779-4091

Funding

This work was supported by NSF under grants 1420882, 1506619, 1708852, 1720701, 1720633, and 1545907.

Notes

The authors declare no competing financial interest.

The supporting code used for the coarse-graining procedure in this work may be accessed at https://github.com/moradza/VOTCA_CRE.

■ ACKNOWLEDGMENTS

The authors acknowledge the use of Blue Waters supercomputing resources at the University of Illinois.

■ REFERENCES

(1) Bates, E. D.; Mayton, R. D.; Ntai, I.; Davis, J. H. CO2 Capture by a Task-Specific Ionic Liquid. *J. Am. Chem. Soc.* **2002**, *124* (6), 926−927.

(2) Vatamanu, J.; Vatamanu, M.; Bedrov, D. Non-Faradaic Energy Storage by Room Temperature Ionic Liquids in Nanoporous Electrodes. *ACS Nano* **2015**, *9* (6), 5999−6017.

(3) Voeltzel, N.; Giuliani, A.; Fillot, N.; Vergne, P.; Joly, L. Nanolubrication by Ionic Liquids: Molecular Dynamics Simulations Reveal an Anomalous Effective Rheology. *Phys. Chem. Chem. Phys.* **2015**, *17* (35), 23226−23235.

(4) Dong, K.; Liu, X.; Dong, H.; Zhang, X.; Zhang, S. Multiscale Studies on Ionic Liquids. *Chem. Rev.* **2017**, *117* (10), 6636−6695.

(5) Hough, W. L.; Smiglak, M.; Rodríguez, H.; Swatloski, R. P.; Spear, S. K.; Daly, D. T.; Pernak, J.; Grisel, J. E.; Carliss, R. D.;

Soutullo, M. D.; et al. The Third Evolution of Ionic Liquids: Active Pharmaceutical Ingredients. *New J. Chem.* **2007**, *31* (8), 1429.
(6) Karplus, M.; McCammon, J. A. Molecular Dynamics Simulations of Biomolecules. *Nat. Struct. Biol.* **2002**, *9* (9), 646−652.
(7) Wendler, K.; Zahn, S.; Dommert, F.; Berger, R.; Holm, C.; Kirchner, B.; Delle Site, L. Locality and Fluctuations: Trends in Lmidazolium-Based Ionic Liquids and Beyond. *J. Chem. Theory Comput.* **2011**, *7* (10), 3040−3044.
(8) Mendonça, A. C. F.; Malfreyt, P.; Pádua, A. A. H. Interactions and Ordering of Ionic Liquids at a Metal Surface. *J. Chem. Theory Comput.* **2012**, *8* (9), 3348−3355.
(9) Feng, G.; Jiang, D.; Cummings, P. T. Curvature Effect on the Capacitance of Electric Double Layers at Ionic Liquid/Onion-like Carbon Interfaces Curvature Effect on the Capacitance of Electric Double Layers at Ionic Liquid/Onion-like Carbon Interfaces. *J. Chem. Theory Comput.* **2012**, *8* (Md), 1058−1063.
(10) Fileti, E. E.; Chaban, V. V. Imidazolium Ionic Liquid Helps to Disperse Fullerenes in Water. *J. Phys. Chem. Lett.* **2014**, *5* (11), 1795−1800.
(11) Singh, R.; Monk, J.; Hung, F. R. Heterogeneity in the Dynamics of the Ionic Liquid [BMIM+][PF6-] Confined in a Slit Nanopore. *J. Phys. Chem. C* **2011**, *115* (33), 16544−16554.
(12) Zhang, Y.; Maginn, E. J. Direct Correlation between Ionic Liquid Transport Properties and Ion Pair Lifetimes: A Molecular Dynamics Study. *J. Phys. Chem. Lett.* **2015**, *6* (4), 700−705.
(13) Shah, J. K.; Brennecke, J. F.; Maginn, E. J. Thermodynamic Properties of the Ionic Liquid 1-n-Butyl-3-Methylimidazolium Hexafluorophosphate from Monte Carlo Simulations. *Green Chem.* **2002**, *4* (2), 112−118.
(14) Izvekov, S.; Voth, G. A. A Multiscale Coarse-Graining Method for Biomolecular Systems. *J. Phys. Chem. B* **2005**, *109* (7), 2469−2473.
(15) Wang, Y.; Voth, G. A. Unique Spatial Heterogeneity in Ionic Liquids. *J. Am. Chem. Soc.* **2005**, *127* (35), 12192−12193.
(16) Wang, Y.; Feng, S.; Voth, G. A. Transferable Coarse-Grained Models for Ionic Liquids. *J. Chem. Theory Comput.* **2009**, *5* (4), 1091−1098.
(17) Wang, Y. T.; Izvekov, S.; Yan, T. Y.; Voth, G. A. Multiscale Coarse-Graining of Ionic Liquids. *J. Phys. Chem. B* **2006**, *110* (8), 3564−3575.
(18) Del Pópolo, M. G.; Voth, G. A. On the Structure and Dynamics of Ionic Liquids. *J. Phys. Chem. B* **2004**, *108* (5), 1744−1752.
(19) Salanne, M.; Rotenberg, B.; Naoi, K.; Kaneko, K.; Taberna, P.-L.; Grey, C. P.; Dunn, B.; Simon, P. Efficient Storage Mechanisms for Building Better Supercapacitors. *Nat. Energy* **2016**, *1* (6), 16070.
(20) Kondrat, S.; Wu, P.; Qiao, R.; Kornyshev, A. Accelerating Charging Dynamics in Sub-Nanometer Pores. *Nat. Mater.* **2014**, *13*, 387−393.
(21) Chaban, V. V.; Maciel, C.; Fileti, E. E. Does the Like Dissolves Like Rule Hold for Fullerene and Ionic Liquids? *J. Solution Chem.* **2014**, *43* (6), 1019−1031.
(22) Vatamanu, J.; Bedrov, D. Capacitive Energy Storage: Current and Future Challenges. *J. Phys. Chem. Lett.* **2015**, *6* (18), 3594−3609.
(23) Merlet, C.; Rotenberg, B.; Madden, P.; Salanne, M. Computer Simulations of Ionic Liquids at Electrochemical Interfaces. *Phys. Chem. Chem. Phys.* **2013**, *15*, 15781−15792.
(24) Izvekov, S.; Voth, G. A. Multiscale Coarse-Graining of Mixed Phospholipid/Cholesterol Bilayers. *J. Chem. Theory Comput.* **2006**, *2* (3), 637−648.
(25) Shi, Q.; Izvekov, S.; Voth, G. A. Mixed Atomistic and Coarse-Grained Molecular Dynamics: Simulation of a Membrane-Bound Ion Channel. *J. Phys. Chem. B* **2006**, *110* (31), 15045−15048.
(26) Vicatos, S.; Roca, M.; Warshel, A. Effective Approach for Calculations of Absolute Stability of Proteins Using Focused Dielectric Constants. *Proteins: Struct., Funct., Genet.* **2009**, *77* (3), 670−684.
(27) Chaimovich, A.; Shell, M. S. Coarse-Graining Errors and Numerical Optimization Using a Relative Entropy Framework. *J. Chem. Phys.* **2011**, *134* (9), 094112.
(28) Chaimovich, A.; Shell, M. S. Relative Entropy as a Universal Metric for Multiscale Errors. *Phys. Rev. E - Stat. Nonlinear, Soft Matter Phys.* **2010**, *81* (6), 1−4.
(29) Noid, W. G.; Liu, P.; Wang, Y.; Chu, J.-W.; Ayton, G. S.; Izvekov, S.; Andersen, H. C.; Voth, G. A. The Multiscale Coarse-Graining Method. II. Numerical Implementation for Coarse-Grained Molecular Models. *J. Chem. Phys.* **2008**, *128* (24), 244115.
(30) Dunn, N. J. H.; Foley, T. T.; Noid, W. G. Van Der Waals Perspective on Coarse-Graining: Progress toward Solving Representability and Transferability Problems. *Acc. Chem. Res.* **2016**, *49* (12), 2832−2840.
(31) Lyubartsev, A. P.; Laaksonen, A. Calculation of Effective Interaction Potentials from Radial Distribution Functions: A Reverse Monte Carlo Approach. *Phys. Rev. E: Stat. Phys., Plasmas, Fluids, Relat. Interdiscip. Top.* **1995**, *52* (4), 3730−3737.
(32) Reith, D.; Pütz, M.; Müller-Plathe, F. Deriving Effective Mesoscale Potentials from Atomistic Simulations. *J. Comput. Chem.* **2003**, *24* (13), 1624−1636.
(33) Mullinax, J. W.; Noid, W. G. Extended Ensemble Approach for Deriving Transferable Coarse-Grained Potentials. *J. Chem. Phys.* **2009**, *131* (10), 104110.
(34) Shell, M. S. The Relative Entropy Is Fundamental to Multiscale and Inverse Thermodynamic Problems. *J. Chem. Phys.* **2008**, *129* (14), 144108.
(35) Shen, J. W.; Li, C.; Van Der Vegt, N. F. A.; Peter, C. Transferability of Coarse Grained Potentials: Implicit Solvent Models for Hydrated Ions. *J. Chem. Theory Comput.* **2011**, *7* (6), 1916−1927.
(36) Lafond, P. G.; Izvekov, S. Multiscale Coarse-Graining of Polarizable Models through Force-Matched Dipole Fluctuations. *J. Chem. Theory Comput.* **2016**, *12* (12), 5737−5750.
(37) Srivastava, A.; Voth, G. A. Solvent-Free, Highly Coarse-Grained Models for Charged Lipid Systems. *J. Chem. Theory Comput.* **2014**, *10* (10), 4730−4744.
(38) Spiga, E.; Alemani, D.; Degiacomi, M. T.; Cascella, M.; Dal Peraro, M. Electrostatic-Consistent Coarse-Grained Potentials for Molecular Simulations of Proteins. *J. Chem. Theory Comput.* **2013**, *9* (8), 3515−3526.
(39) McCullagh, P.; Lake, P. T.; McCullagh, M. Deriving Coarse-Grained Charges from All-Atom Systems: An Analytic Solution. *J. Chem. Theory Comput.* **2016**, *12* (9), 4390−4399.
(40) Dong, K.; Zhang, S.; Wang, J. Understanding the Hydrogen Bonds in Ionic Liquids and Their Roles in Properties and Reactions. *Chem. Commun.* **2016**, *52* (41), 6744−6764.
(41) Saielli, G.; Bagno, A.; Wang, Y. Insights on the Isotropic-to-Smectic A Transition in Ionic Liquid Crystals from Coarse-Grained Molecular Dynamics Simulations: The Role of Microphase Segregation. *J. Phys. Chem. B* **2015**, *119* (9), 3829−3836.
(42) Essmann, U.; Perera, L.; Berkowitz, M. L.; Darden, T.; Lee, H.; Pedersen, L. G. A Smooth Particle Mesh Ewald Method. *J. Chem. Phys.* **1995**, *103* (19), 8577−8593.
(43) Hayes, R.; Warr, G. G.; Atkin, R. Structure and Nanostructure in Ionic Liquids. *Chem. Rev.* **2015**, *115* (13), 6357−6426.
(44) Araque, J. C.; Hettige, J. J.; Margulis, C. J. Modern Room Temperature Ionic Liquids, a Simple Guide to Understanding Their Structure and How It May Relate to Dynamics. *J. Phys. Chem. B* **2015**, *119* (40), 12727−12740.
(45) Fajardo, O. Y.; Bresme, F.; Kornyshev, A. A.; Urbakh, M. Electrotunable Friction with Ionic Liquid Lubricants: How Important Is the Molecular Structure of the Ions? *J. Phys. Chem. Lett.* **2015**, *6* (20), 3998−4004.
(46) Merlet, C.; Salanne, M.; Rotenberg, B.; Madden, P. A. Imidazolium Ionic Liquid Interfaces with Vapor and Graphite: Interfacial Tension and Capacitance from Coarse-Grained Molecular Simulations. *J. Phys. Chem. C* **2011**, *115* (33), 16613−16618.
(47) Yoo, B.; Zhu, Y.; Maginn, E. J. Molecular Mechanism of Ionic-Liquid-Induced Membrane Disruption: Morphological Changes to Bilayers, Multilayers, and Vesicles. *Langmuir* **2016**, *32* (21), 5403−5411.

DOI: 10.1021/acs.jctc.7b01293
J. Chem. Theory Comput. 2018, 14, 3252−3261

(48) Bhargava, B. L.; Devane, R.; Klein, M. L.; Balasubramanian, S.; Palleau, P.; Fischer, H. E.; Cuello, G. J.; Johnson, M.; Melin, P.; Zanchi, D.; et al. Nanoscale Organization in Room Temperature Ionic Liquids: A Coarse Grained Molecular Dynamics Simulation Study. *Soft Matter* **2007**, *3* (11), 1395.
(49) Bhargava, B. L.; Klein, M. L. Formation of Micelles in Aqueous Solutions of a Room Temperature Ionic Liquid: A Study Using Coarse Grained Molecular Dynamics. *Mol. Phys.* **2009**, *107* (4−6), 393−401.
(50) Wang, Y.-L.; Lyubartsev, A.; Lu, Z.-Y.; Laaksonen, A. Multiscale Coarse-Grained Simulations of Ionic Liquids: Comparison of Three Approaches to Derive Effective Potentials. *Phys. Chem. Chem. Phys.* **2013**, *15* (20), 7701.
(51) Bhargava, B. L.; Devane, R.; Klein, M. L.; Balasubramanian, S. Nanoscale Organization in Room Temperature Ionic Liquids: A Coarse Grained Molecular Dynamics Simulation Study. *Soft Matter* **2007**, *3* (11), 1395.
(52) Roy, D.; Maroncelli, M. An Improved Four-Site Ionic Liquid Model. *J. Phys. Chem. B* **2010**, *114* (39), 12629−12631.
(53) Roy, D.; Patel, N.; Conte, S.; Maroncelli, M. Dynamics in an Idealized Ionic Liquid Model. *J. Phys. Chem. B* **2010**, *114* (25), 8410−8424.
(54) Merlet, C.; Salanne, M.; Rotenberg, B. New Coarse-Grained Models of Imidazolium Ionic Liquids for Bulk and Interfacial Molecular Simulations. *J. Phys. Chem. C* **2012**, *116* (14), 7687−7693.
(55) Ishizuka, R.; Matubayasi, N. Self-Consistent Determination of Atomic Charges of Ionic Liquid through a Combination of Molecular Dynamics Simulation and Density Functional Theory. *J. Chem. Theory Comput.* **2016**, *12* (2), 804−811.
(56) Roy, D.; Maroncelli, M. Dynamics in an Idealized Ionic Liquid Model. *J. Phys. Chem. B* **2012**, *116* (20), 5951−5970.
(57) Wu, D.; Kofke, D. A. Phase-Space Overlap Measures. I. Fail-Safe Bias Detection in Free Energies Calculated by Molecular Simulation Phase-Space Overlap Measures. I. Fail-Safe Bias Detection in Free Energies. *J. Chem. Phys.* **2005**, *123* (5), 054103.
(58) Shell, M. S. The Relative Entropy Is Fundamental to Multiscale and Inverse Thermodynamic Problems. *J. Chem. Phys.* **2008**, *129* (14), 144108.
(59) Wang, H.; Junghans, C.; Kremer, K. Comparative Atomistic and Coarse-Grained Study of Water: What Do We Lose by Coarse-Graining? *Eur. Phys. J. E: Soft Matter Biol. Phys.* **2009**, *28* (2), 221−229.
(60) Wang, Y.; Izvekov, S.; Yan, T.; Voth, G. A. Multiscale Coarse-Graining of Ionic Liquids †. *J. Phys. Chem. B* **2006**, *110* (8), 3564−3575.
(61) Dunn, N. J. H.; Noid, W. G. Bottom-up Coarse-Grained Models That Accurately Describe the Structure, Pressure, and Compressibility of Molecular Liquids. *J. Chem. Phys.* **2015**, *143* (24), 243148.
(62) Bertsekas, D. P. *Nonlinear Programming*; Athena Scientific: Nashua, NH, 1999.
(63) Rühle, V.; Junghans, C.; Lukyanov, A.; Kremer, K.; Andrienko, D. Versatile Object-Oriented Toolkit for Coarse-Graining Applications. *J. Chem. Theory Comput.* **2009**, *5* (12), 3211−3223.
(64) Mashayak, S. Y.; Jochum, M. N.; Koschke, K.; Aluru, N. R.; Rühle, V.; Junghans, C. Relative Entropy and Optimization-Driven Coarse-Graining Methods in VOTCA. *PLoS One* **2015**, *10* (7), e0131754.
(65) Keblinski, P.; Eggebrecht, J.; Wolf, D.; Phillpot, S. R. Molecular Dynamics Study of Screening in Ionic Fluids. *J. Chem. Phys.* **2000**, *113* (1), 282−291.
(66) Gebbie, M. A.; Dobbs, H. A.; Valtiner, M.; Israelachvili, J. N. Long-Range Electrostatic Screening in Ionic Liquids. *Proc. Natl. Acad. Sci. U. S. A.* **2015**, *112* (24), 7432−7437.
(67) Gebbie, M. A.; Valtiner, M.; Banquy, X.; Fox, E. T.; Henderson, W. A.; Israelachvili, J. N. Ionic Liquids Behave as Dilute Electrolyte Solutions. *Proc. Natl. Acad. Sci. U. S. A.* **2013**, *110* (24), 9674−9679.
(68) Peter, C.; Kremer, K. Multiscale Simulation of Soft Matter Systems − from the Atomistic to the Coarse-Grained Level and Back. *Soft Matter* **2009**, *5* (22), 4357.
(69) Rudzinski, J. F.; Lu, K.; Milner, S. T.; Maranas, J. K.; Noid, W. G. Extended Ensemble Approach to Transferable Potentials for Low-Resolution Coarse-Grained Models of Ionomers. *J. Chem. Theory Comput.* **2017**, *13* (5), 2185−2201.
(70) Dunn, N. J. H.; Foley, T. T.; Noid, W. G. Van Der Waals Perspective on Coarse-Graining: Progress toward Solving Representability and Transferability Problems. *Acc. Chem. Res.* **2016**, *49* (12), 2832−2840.
(71) Dunn, N. J. H.; Noid, W. G. Bottom-up Coarse-Grained Models That Accurately Describe the Structure, Pressure, and Compressibility of Molecular Liquids. *J. Chem. Phys.* **2015**, *143* (24), 243148.
(72) Gu, Z.; Brennecke, J. F. Volume Expansivities and Isothermal Compressibilities of Imidazolium and Pyridinium-Based Ionic Liquids. *J. Chem. Eng. Data* **2002**, *47* (2), 339−345.
(73) He, Y.; Qiao, R.; Vatamanu, J.; Borodin, O.; Bedrov, D.; Huang, J.; Sumpter, B. G. Importance of Ion Packing on the Dynamics of Ionic Liquids during Micropore Charging. *J. Phys. Chem. Lett.* **2016**, *7* (1), 36−42.
(74) Pean, C.; Daffos, B.; Rotenberg, B.; Levitz, P.; Haefele, M.; Taberna, P. L.; Simon, P.; Salanne, M. Confinement, Desolvation, and Electrosorption Effects on the Diffusion of Ions in Nanoporous Carbon Electrodes. *J. Am. Chem. Soc.* **2015**, *137* (39), 12627−12632.
(75) Kondrat, S.; Wu, P.; Qiao, R.; Kornyshev, A. A. Accelerating Charging Dynamics in Subnanometre Pores. *Nat. Mater.* **2014**, *13* (4), 387−393.
(76) Davtyan, A.; Dama, J. F.; Voth, G. A.; Andersen, H. C. Dynamic Force Matching: A Method for Constructing Dynamical Coarse-Grained Models with Realistic Time Dependence. *J. Chem. Phys.* **2015**, *142* (15), 154104.
(77) Davtyan, A.; Voth, G. A.; Andersen, H. C. Dynamic Force Matching: Construction of Dynamic Coarse-Grained Models with Realistic Short Time Dynamics and Accurate Long Time Dynamics. *J. Chem. Phys.* **2016**, *145* (22), 224107.
(78) Trément, S.; Schnell, B.; Petitjean, L.; Couty, M.; Rousseau, B. Conservative and Dissipative Force Field for Simulation of Coarse-Grained Alkane Molecules: A Bottom-up Approach. *J. Chem. Phys.* **2014**, *140* (13), 134113.
(79) Markutsya, S.; Lamm, M. H. A Coarse-Graining Approach for Molecular Simulation That Retains the Dynamics of the All-Atom Reference System by Implementing Hydrodynamic Interactions. *J. Chem. Phys.* **2014**, *141* (17), 174107.
(80) Tokuda, H.; Hayamizu, K.; Ishii, K.; Susan, M. A. B. H.; Watanabe, M. Physicochemical Properties and Structures of Room Temperature Ionic Liquids. 1. Variation of Anionic Species. *J. Phys. Chem. B* **2004**, *108* (42), 16593−16600.

DOI: 10.1021/acs.jctc.7b01293
J. Chem. Theory Comput. 2018, 14, 3252−3261